Journal of Computational Physics 409 (2020) 109325

Contents lists available at ScienceDirect

Journal of Computational Physics

www.elsevier.com/locate/jcp

Linear stability eigenmodal analysis for steady and temporally periodic boundary-layer flow configurations using a velocity-vorticity formulation

Scott Morgan, Christopher Davies *

School of Mathematics, Cardiff University, Senghennydd Road, Cardiff, CF24 4AG, UK

ARTICLE INFO

Article history:
Received 5 September 2019
Received in revised form 13 January 2020
Accepted 12 February 2020
Available online 17 February 2020

Keywords:
Hydrodynamic stability
Boundary layer
Vorticity method
Normal mode
Floquet mode
Numerical solution

ABSTRACT

A novel solution procedure is presented for undertaking the linear stability eigenmodal analysis of two and three dimensional steady and time-periodic boundary-layer flow configurations. A velocity-vorticity formulation of the governing equations is deployed, together with a numerical discretisation that utilises a version of the Chebyshev-tau method. The required linear operators are applied in an integrated form to the Chebyshev series representations, instead of the more commonly used differential form. No-slip conditions are imposed in a fully consistent manner using integral constraints on the vorticity. The chosen numerical methods culminate in matrix equations which can be constructed in a relatively simple manner. These are then solved using the eigenvalue routines available in standard software libraries for linear algebra.

Validation is provided against previously published results for two distinct cases. Firstly, for the steady boundary layer formed above a disk of infinite extent that rotates with a constant angular velocity. Secondly, for the semi-infinite time-periodic Stokes layer that is driven by the oscillatory motion of a flat plate. New results are then presented for the oscillatory boundary layer that forms above a disk that rotates with a rate that is periodically modulated. This configuration can be construed as providing a canonical example of a three-dimensional temporally periodic boundary layer. Its stability is examined here for the first time, with a Floquet analysis conducted by combining the solution methods that were developed for the other two cases.

1. Introduction

Linear stability analysis plays an important part in the study of many boundary-layer flow configurations, where it can help to elucidate the mechanisms involved in the development of disturbances during the transition to turbulence [29]. This paper is concerned with the description and application of a novel procedure for solving the linear stability eigenvalue problems that arise for two and three dimensional steady and temporally periodic boundary layers. Although we will limit our illustration of the applications to a small number of canonical incompressible flow configurations, it should be noted that the procedure is independent of many of the specific features of the base flow. It is in principle applicable to a wide range of steady or temporally periodic, two or three dimensional externally configured boundary layers.

* Corresponding author.
E-mail address: DaviesC9@cardiff.ac.uk (C. Davies).

https://doi.org/10.1016/j.jcp.2020.109325
0021-9991/

Linear stability analyses may be embarked upon from either a primitive variable or a vorticity-based formulation of the Navier-Stokes equations. These can then be used to yield governing equations for the development of infinitesimal perturbations to a steady or temporally periodic boundary layer. One of the most well-known examples of this process is the derivation which leads to the Orr-Sommerfeld equation and its associated eigenvalue problem. The study of this particular stability equation can be traced back for more than a century [26,31]. For example, Heisenberg [18] used its approximated solutions to provide one of the first arguments to demonstrate that, somewhat counter-intuitively, viscosity could have a destabilising effect on the development of flow disturbances. The Orr-Sommerfeld equation may be deduced from the vorticity equation for the linearised evolution of two dimensional disturbances within a steady unidirectional shear flow, once a normal-mode structure has been assumed. This genealogy is not immediately apparent from an inspection of the equation, since it takes the form of a fourth-order differential equation, rather than a second-order equation, where the vorticity perturbation has been eliminated using a representation in terms of the wall-normal velocity.

An alternative to solving the Orr-Sommerfeld equation is to utilise a coupled system of two second-order differential equations, which directly involve both the vorticity and the wall-normal velocity perturbations. However, this introduces the apparent technical difficulty that there are no boundary conditions that can be applied to the vorticity at the locations of flow-confining walls. Instead, when carrying things over from the more usual fourth-order formulation, it might at first seem that all such conditions must be applied to the wall-normal velocity alone. In this paper we will illustrate how this is not the case and show that integral constraints can be used to provide appropriate conditions on the vorticity. The enforcement of these integral constraints is fully equivalent to the imposition of no-slip conditions at the appropriate boundary of the flow. Adopting an approach that involves the use of vorticity equations in conjunction with integral constraints, we are able to incorporate configurations that involve time-periodic and three dimensional basic states. Thus we move beyond the scope of the relatively straightforward shear flows that can be treated by solving the Orr-Sommerfeld equation. These merely provide the most elementary cases where our methods may be deployed.

It will be seen that the approach that we have taken involves the specialised application of various ideas that were originally developed by Davies and Carpenter [11] in the broader context of a vorticity-based formulation of the Navier-Stokes equations. This formulation has been extensively utilised to conduct numerical simulations of boundary-layer disturbance development (for three recent examples, see [34–36]). In the current study, the same vorticity-based system of governing equations, together with its associated boundary conditions and integral constraints, is restricted to cases where the base flow exhibits a sufficient measure of spatial uniformity to allow the perturbations to be simplified by prescribing them to have a suitable normal-mode or Floquet-mode structure. This ensures that the stability problem can be cast in the form of an eigenvalue problem that only requires the determination of the wall-normal spatial variation of the disturbance flow fields.

Our numerical discretisation utilises a version of the Chebyshev-tau method, in a scheme that is broadly similar to what has been successfully deployed in a number of previous investigations [5–7,9,11]. A central feature of this scheme is that the governing equations for the perturbations are integrated indefinitely to eliminate derivatives. This leads to matrix representations that can be constructed in a relatively simple fashion when the flow variables are approximated using truncated Chebyshev series. More importantly, it will be shown that the employment of a tau-method, in conjunction with the integrated forms of the appropriate linear operators, readily facilitates the implementation of the previously mentioned integral constraints on the vorticity that are used to enforce the no-slip conditions.

Much of the present paper will be taken up with the elaboration and elucidation of the very brief and preliminary outline of our novel solution procedure that has just been given. The formulation of the governing equations and the numerical discretisation method, together with an illustrative selection of numerical results, will all be described later in a more comprehensive manner. But before this, we first provide a short review of the fundamental flow configurations to which we have applied our novel solution procedures, making a few selected references to the relevant research literature.

1.1. The steady rotating disk boundary layer

The steady rotating disk boundary layer is formed when a flat solid surface is rotated in an unbounded incompressible fluid, with a constant angular velocity about an axis which is normal to that surface. The earliest comprehensive studies of its local linear stability were undertaken by Mack [22] and Malik [23], mainly with a view to elucidating the instability mechanisms for the flow over a swept wing. This seemingly obscure motivation was first proposed by Gregory et al. [16], who showed that both configurations can exhibit the same crossflow instability mechanism, which leads to the formation of crossflow vortices. As a consequence, the stability behaviour of the rotating disk flow has been investigated both as an approximation to the flow over a swept wing and as a canonical example for three dimensional boundary layers. The latter nomination is apt because there is the advantage that the rotating disk configuration admits an exact similarity solution to the Navier-Stokes equations [37]. Taken together with the fact that the rotating disk is relatively easy to work with experimentally, in comparison with the swept wing, this has inspired a large number of stability studies over the past few decades. A representative sample of these can be found in [1,7,8,15,19,32]. A relatively recent review is given by Lingwood and Alfredsson [20].

There are three distinct types of instability that are known to be present in the rotating disk boundary layer. The crossflow instability or type I mode was originally discovered by Gregory et al. [16]. This instability is fundamentally inviscid in nature. As has already been mentioned, the same instability mechanism arises for flows over swept wings, but it can also

occur for other boundary layer flows around a variety of rotating objects. For disturbances which are stationary with respect to the disk surface, the type I mode is the most unstable of the three types of instability, in the sense that it sets in at the lowest Reynolds number.

The second mode of instability, labelled as the type II mode, can be distinguished from the type I mode by its viscous nature and its origin in streamwise curvature and Coriolis effects. In the neutral curves presented by Malik [23], the type I and type II instabilities can be clearly identified as being separate. Both of them may occur as either a stationary disturbance or as a wave that travels relative to the disk surface. Mack [22] mentions a third mode, now known as the type III mode, which propagates towards the disk centre but is spatially damped. The significance of this mode was not immediately appreciated and, for a long period of time, almost all attention was paid to the stationary form of the type I instability. The importance of travelling instabilities in the spatio-temporal structure of the disturbance evolution for the rotating disk flow was not realised until Lingwood's [19] discovery of a local absolute instability. This was shown to arise as the result of a coalescence between the type I and type III modes.

In the present paper, the validation of our numerical solution procedures will initially focus on the replication of previously determined characteristics for the onset of instability for stationary forms of disturbance in the steady rotating disk boundary layer. No attempt will be made here to duplicate any of the features pertaining to the onset of the absolute form of instability, although these can also be addressed using our solution methods [25].

1.2. The semi-infinite Stokes layer

Temporally periodic oscillatory flows occur in many types of physical and physiological processes. For example, Womersley [38] shows that high frequency oscillatory blood flow in an artery can be modelled by invoking a Stokes layer adjacent to the wall, along with a region of inviscid flow at the centre of the artery. To provide some further stringent testing of our methods, for an example of a temporally-periodic two dimensional boundary layer, we will consider the stability of the flow in the semi-infinite Stokes layer. This is the flow that is generated when a flat plate oscillates within its own plane, beneath an otherwise unbounded expanse of fluid. It may be described by an exact analytic solution of the Navier-Stokes equations, which has led to it being construed as the most elementary prototype for externally configured oscillatory flows.

Extensive reviews concerned with the unstable behaviour of disturbances in the semi-infinite Stokes layer and other closely related oscillatory boundary layers are readily available within the literature. An early account given by Davis [13] contains details of the problem formulation, and several authors including Hall [17], Blennerhassett and Bassom [3,4], Thomas et al. [33] and Ramage [27] have built upon this to investigate the onset and nature of the instability. A review of the common methods for analysing the stability of oscillatory boundary-layer flows, including quasi-static approximations and the use of linearised direct numerical simulations, is provided by Thomas et al. [35] and so will not be repeated here. Our choice of the problem formulation will be similar to that of Hall [17] and Blennerhassett and Bassom [3,4], which is taken within the framework of Floquet theory. Ramage [27] gives an overview of Floquet theory and its applicability to the linear stability problem that we shall consider here, the details of which are beyond the scope of this primarily methods-based paper. The reader is referred to the reference for further discussion. The stability results that we have determined will be carefully compared against those that were reported by Blennerhassett and Bassom [3,4] and Ramage [27].

1.3. The periodically-modulated rotating disk boundary layer

The final flow configuration that is to be considered involves a novel combination of the features of the two examples that have just been described in sections 1.1 and 1.2. We will examine the Floquet stability properties of a three dimensional oscillatory rotating disk boundary-layer flow. This is formed above a surface which rotates with a periodically modulated angular velocity, about a fixed axis that is perpendicular to the surface. As with the cases for a steadily rotating disk and the oscillatory flat plate motion, the fluid extends indefinitely above the moving surface that generates the boundary layer, while the surface itself is taken to have no delimiting edges.

Aside from being of fundamental interest in its own right, motivation for the incorporation of a modulated rotation rate stems from the work reported in Thomas et al. [33]. It was shown that for steady unidirectional wall-bounded shear flows, the addition of relatively small amounts of temporal oscillation can lead to stabilising effects. The examples of plane Poiseuille flow and Hagen-Poiseuille flow were considered, where aligned oscillatory wall motions could be utilised to introduce a time-modulated component into the base-flow. The latter of these two flows is known to be linearly stable, even without any oscillatory modification. Thus plane Poiseuille flow might be construed as being the most interesting case, since it was found that for certain frequencies of the wall oscillation, the critical Reynolds number for the onset of instability could be nearly doubled. This held out the prospect of applications to externally configured boundary-layer flows, where it is conceivable that the same kind of base flow modification could yield stabilisations that delay laminar-turbulent transition. Moreover, it has already been shown that the introduction of an oscillatory velocity component into the Blasius boundary layer, albeit with a spatial rather than a temporal periodicity, can suppress the growth of streaks. See, for example, the study by Ricco [28]. With all of this in mind, we have sought to establish whether any favourable stability effects could also be found for the rotating disk boundary layer. In the current paper, we will briefly present some illustrative results that demonstrate that stabilising effects can in fact be obtained. A more complete discussion and a much fuller parametric study are given by Morgan [25], which will be separately reported upon elsewhere.

The periodically modulated rotating disk configuration also has applications in electrochemical engineering. As discussed by Bard and Faulkner [2], the steady rotating disk electrode provides a convenient configuration for hydrodynamic voltammetry, where convection of an analyte controlled by the rotation is designed to increase the rate of mass transport of ions at an electrode surface. This technique is commonly used for electroplating. Schwartz et al. [30] discuss the favourable effects that can be achieved for the mass transfer if the disk is rotated with a periodic variation of its angular velocity.

Now that we have given a brief description of the flow configurations to which our solution procedures will be applied, the paper proceeds as follows. In section 2 we present the solution procedure for time-independent three dimensional boundary layer flows, using the example of the steady rotating disk flow. Section 3 describes the extension of the methods to time-dependent boundary layers by considering the semi-infinite Stokes layer, and introduces the formulation that is needed to undertake an analysis based upon Floquet theory. Section 4 then extends the scope of the Floquet theory solution methods to three dimensions. These are applied to the periodically-modulated rotating disk flow configuration, which to the best of the authors' knowledge has not previously been studied. Concluding remarks are given in section 5.

2. Linear stability of steady three dimensional flow configurations

To begin the account of our solution procedure, we consider an illustrative example for a steady three dimensional boundary layer. We present our velocity-vorticity formulation of the linearised Navier-Stokes equations, together with the chosen numerical discretisation methods, for the specific case of the steady rotating disk boundary layer. This means that it is natural to use a cylindrical polar system, but the general approach is applicable to other prescriptions for the co-ordinates, provided the semi-infinite region of fluid that needs to be considered remains bounded by a surface wall that can be modelled as being of unlimited extent.

A number of distinct approaches have previously been taken to conduct a linear stability analysis of the rotating disk boundary layer [1,7,8,19,23]. These have all used either primitive variables or a formulation that represents a three dimensional generalisation of the Orr-Sommerfeld equation. In the latter case, the usual fourth-order equation for the wall-normal velocity component is modified and directly coupled to a second-order equation for the wall-normal component of the vorticity. A variety of numerical discretisation methods have been applied, ranging over Runge-Kutta integration, high-order finite differences, Chebyshev collocation and Chebyshev tau methods. The results that were obtained in these previous studies have been used to validate our own numerical methods.

2.1. Velocity-vorticity formulation for the perturbation analysis

There is an exact similarity solution to the Navier-Stokes equations for the laminar base flow over a disk of notionally infinite radius, which rotates with a constant angular velocity [37]. If the dimensional quantities of kinematic viscosity and angular velocity are denoted by ν^* and Ω^* respectively, then it is possible to define a boundary layer thickness $\delta^* = \sqrt{\nu^*/\Omega^*}$ that remains constant throughout the flow. This may be utilised as a reference for the non-dimensionalisation of length scales. A local velocity scaling is obtained by using the circumferential disk velocity $r_L^*\Omega^*$ at some chosen dimensional reference radius r_L^*, while the time may be scaled with $\delta^*/(\Omega^* r_L^*)$. The associated locally-defined Reynolds number is

$$R = \frac{\left(r_L^*\Omega^*\right)\,\delta^*}{\nu^*} = \frac{r_L^*}{\delta^*} = r_L\,, \tag{1}$$

which can be interpreted as designating a non-dimensional radius on the disk. Using these scalings, the similarity solution for the base flow in cylindrical polar co-ordinates (r,θ,z) can be written in the form

$$\mathbf{U}_B(r,z) = \left(\frac{r}{R}F(z), \frac{r}{R}G(z), \frac{1}{R}H(z)\right)\,. \tag{2}$$

The profile functions F, G, H may readily be determined from the numerical solution of a set of coupled ordinary differential equations. These are given by the steady version of the equations (38) that are stated later in Section 4, for the more general case where there is a time-varying rotation rate. The solid surface of the rotating disk is taken to be at $z = 0$.

Disturbances from the basic-state velocity and vorticity fields are introduced by decomposing the total flow as

$$\mathbf{U}(r,\theta,z,t) = \mathbf{U}_B(r,z) + \mathbf{u}(r,\theta,z,t), \qquad (\nabla\times\mathbf{U})\,(r,\theta,z,t) = (\nabla\times\mathbf{U}_B)\,(r,z) + \boldsymbol{\xi}(r,\theta,z,t)\,, \tag{3}$$

where $\mathbf{u} = (u_r, u_\theta, w)$ and $\boldsymbol{\xi} = \nabla\times\mathbf{u} = (\xi_r, \xi_\theta, \xi_z)$ represent the perturbation quantities. Following the formulation first presented by Davies and Carpenter [11], we identify the three *primary* flow-field variables as $\{\xi_r, \xi_\theta, w\}$ and consider the remaining three variables $\{u_r, u_\theta, \xi_z\}$ to be *secondary*. In the frame of reference that rotates with the disk, the system of governing equations for the primary variables is

$$\frac{\partial \xi_r}{\partial t} + \frac{1}{r}\frac{\partial N_z}{\partial \theta} - \frac{\partial N_\theta}{\partial z} - \frac{2}{R}\left(\xi_\theta + \frac{\partial w}{\partial r}\right) = \frac{1}{R}\left[\left(\nabla^2 - \frac{1}{r^2}\right)\xi_r - \frac{2}{r^2}\frac{\partial \xi_\theta}{\partial \theta}\right] \tag{4a}$$

$$\frac{\partial \xi_\theta}{\partial t} + \frac{\partial N_r}{\partial z} - \frac{\partial N_z}{\partial r} + \frac{2}{R}\left(\xi_r - \frac{1}{r}\frac{\partial w}{\partial \theta}\right) = \frac{1}{R}\left[\left(\nabla^2 - \frac{1}{r^2}\right)\xi_\theta + \frac{2}{r^2}\frac{\partial \xi_r}{\partial \theta}\right] \tag{4b}$$

$$\nabla^2 w = \frac{1}{r}\left(\frac{\partial \xi_r}{\partial \theta} - \frac{\partial (r\xi_\theta)}{\partial r}\right), \tag{4c}$$

where

$$\mathbf{N} = (N_r, N_\theta, N_z) = (\nabla \times \mathbf{U}_B) \times \mathbf{u} + \boldsymbol{\xi} \times \mathbf{U}_B + \underbrace{\boldsymbol{\xi} \times \mathbf{u}}_{\text{nonlinear}} \tag{5}$$

and the secondary variables may all be eliminated by explicitly expressing them in terms of integrals of the primary variables across the boundary layer

$$u_r = -\int_z^\infty \left(\xi_\theta + \frac{\partial w}{\partial r}\right) dz', \qquad u_\theta = \int_z^\infty \left(\xi_r - \frac{1}{r}\frac{\partial w}{\partial \theta}\right) dz', \qquad \xi_z = \frac{1}{r}\int_z^\infty \left(\frac{\partial (r\xi_r)}{\partial r} + \frac{\partial \xi_\theta}{\partial \theta}\right) dz'. \tag{6}$$

In the usual manner, ∇^2 represents the Laplacian operator in cylindrical polar coordinates. Subject to some easily accommodated restrictions on the disturbance behaviour in the $z \to \infty$ limit, the system stated above is fully-equivalent to the Navier-Stokes equations in a primitive variables form. For the purposes of the present analysis, a linearisation is performed by simply dropping the term labelled nonlinear in (5).

It may be noted that the transport equations for the vorticity components ξ_r and ξ_θ, as well as the Poisson equation that determines the wall-normal velocity component w, are all second order with respect to the spatial variation. This suggests that for each of these equations, two separate conditions must be imposed in order to fix any putative solution for the wall-normal variation. The enforcement of vanishing conditions upon the primary variables in the far-field as $z \to \infty$ is an obvious choice, given that we are concerned with perturbation quantities. It is also clear that the no-penetration requirement at the disk surface $z = 0$ supplies the appropriate second condition that needs to be applied in conjunction with the Poisson equation for w. However, it is not immediately apparent what second conditions might be associated with the two vorticity transport equations, since nothing can be known in advance about the values taken by the perturbation vorticity components ξ_r and ξ_θ at the surface of the disk. Instead, only the no-slip condition on the velocity components u_r and u_θ can be prescribed. Although these two velocity components are effectively removed from the system of governing equations, having been defined in terms of the primary variables, they must still be allowed to play an essential role in constraining the vorticity evolution. This can be accomplished by simply setting $z = 0$ as the lower limit in the integrals that are used to define them, in order to specify their values at the disk surface. The no-slip conditions on the disk surface can then be cast as integral constraints on the vorticity. Together with the no-penetration condition, these take the form

$$\int_0^\infty \left(\xi_\theta + \frac{\partial w}{\partial r}\right) dz' = 0, \qquad \int_0^\infty \left(\xi_r - \frac{1}{r}\frac{\partial w}{\partial \theta}\right) dz' = 0, \qquad w(0) = 0. \tag{7}$$

2.2. Parallel flow approximation and normal-mode decomposition

The so-called parallel flow approximation [20,24] for the rotating disk configuration is applied in order to simplify the governing equations for the linearised disturbances, making them homogeneous with respect to the radial co-ordinate. It amounts to selecting the base flow at one given radial position and replicating this at all other locations, by artificially setting $r = R$ in the coefficients that appear in the perturbation equations. This facilitates the use of a normal-mode representation for the radial variation. Since there is already an homogeneity in time, because the base flow is steady, together with an azimuthal periodicity due to cylindrical geometry, the velocity and vorticity perturbations can then be chosen to have the normal-mode form

$$\mathbf{u} = \tilde{\mathbf{u}}(z)\, e^{i(\alpha r + n\theta - \omega t)}, \quad \xi = \tilde{\xi}(z)\, e^{i(\alpha r + n\theta - \omega t)}, \tag{8}$$

where α is the radial wavenumber and ω is the temporal frequency. The azimuthal mode number $n = \beta R$ may be compared experimentally with the number of spiral vortices that are found along a cycle around the disk surface. Although the geometry constrains n to be integer-valued, for practical purposes we will do as others have done and treat β, and therefore n, as continuously varying. In addition to applying the parallel flow approximation, we also neglect higher-order terms in governing equations that are $O(1/R^2)$, taking account of the fact that it is also usually assumed that the azimuthal mode number n is $O(R)$. This is required in order to enforce a measure of consistency in the approximation and to ensure compatibility with previous research.

2.3. Wall-normal co-ordinate mapping and Chebyshev series representation

The wall-normal variation of the disturbances is expressed using a mapped co-ordinate, which transforms the semi-infinite physical domain $[0, \infty)$ to the finite computational domain $(0, 1]$. This is specified by setting

$$\eta = \frac{l}{l+z}, \tag{9}$$

where l is an appropriately chosen $O(1)$ stretching factor. The profiles $\tilde{p}$ of the primary perturbation variables are then represented using odd Chebyshev series in the transformed wall-normal co-ordinate. These are taken to have the form

$$\tilde{p}(\eta) = \eta^2 \hat{p}(\eta) = \eta^2 \sum_{k=1}^{M} p_k T_{2k-1}(\eta), \tag{10}$$

where M is the order of the truncation. The incorporation of the additional η^2 factor is convenient because it simplifies the determination of the secondary variables from the primary variables using the integrals defined in (6). It takes account of the fact that transforming between the physical and computational co-ordinates introduces a division by η^2 into the integrands. Inspection of the definitions of the secondary variables also makes it clear that they must be taken to be of the opposite parity to the primary variables, requiring them to be represented using a series of even Chebyshev polynomials. We can thus approximate the profiles $\tilde{s}$ of the secondary variables with series of the form

$$\tilde{s}(\eta) = \sum_{k=1}^{M} s_k \left(T_{2k}(\eta) - T_{2k}(0) \right), \tag{11}$$

where the subtraction of $T_{2k}(0) = (-1)^k$ arises from their definition in terms of integrals across the boundary layer. The secondary variables must automatically vanish when $\eta = 0$, which corresponds to the limit $z \to \infty$. It should be noted that, throughout what follows, the use of a circumflex ($\hat{}$) above a flow variable will indicate that it has been divided by η^2, while a tilde ($\tilde{}$) will be reserved for variables where that is not the case.

2.4. Discretisation of the perturbation equations

Adopting a procedure that is similar to that which has been successfully utilised in a number of previous studies [5–7, 10,11] the linearised governing equations (4) are integrated twice indefinitely with respect to the mapped variable η, after the normal-mode structure (8) has been applied. This yields the following set of equations that determine the variation of the primary flow-field variables across the boundary layer

$$\mathbf{I}_2 \left[-i\omega\hat{\xi}_r + i\beta\hat{N}_z - \frac{2}{R}\left(\hat{\xi}_\theta + i\alpha\hat{w}\right) + \frac{1}{R}\left(\alpha^2+\beta^2\right)\hat{\xi}_r \right] + \frac{1}{l}\mathbf{I}_1\tilde{N}_\theta - \frac{1}{Rl^2}\mathbf{J}\hat{\xi}_r = 0 \tag{12a}$$

$$\mathbf{I}_2 \left[-i\omega\hat{\xi}_\theta - i\alpha\hat{N}_z + \frac{2}{R}\left(\hat{\xi}_r - i\beta\hat{w}\right) + \frac{1}{R}\left(\alpha^2+\beta^2\right)\hat{\xi}_\theta \right] - \frac{1}{l}\mathbf{I}_1\tilde{N}_r - \frac{1}{Rl^2}\mathbf{J}\hat{\xi}_\theta = 0 \tag{12b}$$

$$\mathbf{I}_2 \left(\left\{ \frac{i\alpha}{R} - \alpha^2 - \beta^2 \right\} \hat{w} - i\beta\hat{\xi}_r + i\alpha\hat{\xi}_\theta + \frac{1}{R}\hat{\xi}_\theta \right) + \frac{1}{l^2}\mathbf{J}\hat{w} = 0, \tag{12c}$$

where the integral operators are given by

$$\mathbf{I}_1 f := \int f; \qquad \mathbf{I}_2 f := \iint f; \qquad \mathbf{J}f := \eta^4 f - 2\int \eta^3 f. \tag{13}$$

For the purposes of brevity, we have used a notation that omits any inessential references to the integration variables. It should be mentioned that when the parallel flow approximation is applied to the terms that involve the quantity $\mathbf{N}$, some care is needed to remain consistent. Attention needs to be paid to the stage in the derivation where the replacements $r \to R$ and $\partial/\partial r \to i\alpha$ are made, since these cannot be commuted in every instance.

The matrix representations of the actions of the integration operators on the Chebyshev series take a conveniently simple form. They are all banded and at most pentadiagonal. This follows from the fact that each of the relevant integrals and multiples of the Chebyshev polynomials can be found using successive applications of the recipes

$$\int T_k(\eta)d\eta = \begin{cases} \frac{1}{2(k+1)}T_{k+1}(\eta) - \frac{1}{2(k-1)}T_{|k-1|}(\eta) & k \neq 1 \\ \frac{1}{4}T_2(\eta) & k = 1 \end{cases} \tag{14}$$

and

$$\eta T_k(\eta) = \frac{1}{2}\left(T_{k+1}(\eta) + T_{|k-1|}(\eta) \right).$$

2.5. Secondary variables and the imposition of the no-slip conditions

Referring once more back to (6), it may be observed that the definitions of secondary variables can all be rewritten in the general form

$$\tilde{s} = \int_0^{\eta} \hat{q}\, d\eta' \,, \tag{15}$$

where $\hat{q}$ denotes a linear combination of the primary flow-field profile functions. For example, for the radial velocity component we have

$$\tilde{u}_r(\eta) = l \int_0^{\eta} \left(\hat{\xi}_r + i\alpha \hat{w} \right) d\eta' . \tag{16}$$

When this general form is used in conjunction with the Chebyshev polynomial integration recipe that was stated immediately above, it may be inferred that the Chebyshev coefficients for the secondary variables can be determined from those of the primary variables by simply setting

$$s_k = \frac{1}{4k} \left(q_k - q_{k+1} \right) . \tag{17}$$

This relationship can be deployed to obtain the discretised versions of the previously stated constraints on the vorticity, which must be applied in order to impose the no-slip conditions. These require the vanishing of the radial and azimuthal perturbation velocities at the disk surface, or in other words $\tilde{s}(1) = 0$ for both velocity components, since $\eta = 1$ corresponds to $z = 0$. We can thus derive conditions on the primary variable Chebyshev coefficients that may be arranged into the form

$$\sum_{k=1}^{M} I_k \, q_k = 0, \tag{18}$$

where the fixed constants I_k are given by

$$I_k = \begin{cases} \frac{1}{k} & \text{for even } k \\ \frac{-1}{k-1} & \text{odd } k \end{cases}$$

The integral constraints on the vorticity perturbations, together with the no-penetration condition, which were all previously stated in (7), can now be rewritten in a fully-discretised form as

$$\sum_{k=1}^{M} I_k \left(\xi_{\theta k} + i\alpha w_k \right) = 0, \qquad \sum_{k=1}^{M} I_k \left(\xi_{rk} - i\beta w_k \right) = 0, \qquad \sum_{k=1}^{M} w_k = 0. \tag{19}$$

Use has been made of the parallel flow approximation to eliminate the radial dependence that would otherwise have appeared in the integral constraint on the radial vorticity perturbation. The discrete version of the no-penetration condition is obtained by using the fact that $T_{2k-1}(1) = 1$ for all k to evaluate the Chebyshev series for the wall-normal perturbation velocity at the disk surface.

The three conditions (19) can be readily deployed to close the fully-discretised version of the system of governing equations (12). Setting the combined actions of the indicated linear operators to yield vanishing projections onto the Chebyshev polynomials T_{2k-1} for $k = 2, 3, \ldots M$, we obtain $3(M-1)$ distinct conditions that may be imposed upon the set of $3M$ unknown coefficients $\{\xi_{rk}, \xi_{\theta k}, w_k\}$. However, the same procedure cannot be extended to the case $k = 1$. The results of the operators with respect to the lowest order Chebyshev polynomial are undetermined, since they introduce arbitrary constants of integration and through this an unknown multiple of $T_1(\eta) = \eta$. This indeterminacy can be removed by simply enforcing, instead, the discrete implementations (19) of the two vorticity integral constraints and the no-penetration condition.

The numerical discretisation procedure that has now been outlined amounts to the application of a version of the Chebyshev-tau method. The actions of the linear operators that appear in the discretised equations generate Chebyshev polynomials that have a higher order than those that are included in the truncated Chebychev series approximations. The projections onto these higher order polynomials are conventionally designated as tau-coefficients. Rather than being explicitly set to be zero, they are only presumed to converge to zero, as the order of the Chebyshev series truncation is increased.

2.5.1. Treatment of the base flow product terms

The governing equations (4) contain terms that involve products between the perturbation fields and various quantities that are determined by the base flow. General methods for dealing with such products are discussed in some detail by Bridges and Morris [5], who also present an application to the solution of the Orr-Sommerfeld equation for Poiseuille flow in a planar channel. The central feature is the use of the product formula for Chebyshev polynomials

$$T_j T_k = \frac{1}{2}\left(T_{j+k} + T_{|j-k|}\right). \tag{20}$$

If this is applied to a product between two truncated Chebyshev series

$$U = \frac{U_0}{2} + \sum_{k=1}^{M'} U_k T_k \qquad f = \frac{f_0}{2} + \sum_{k=1}^{M'} f_k T_k \tag{21}$$

then we can obtain the approximation

$$Uf = \sum_{k=1}^{M'} (Uf)_k T_k \,, \tag{22}$$

where

$$(Uf)_k = \frac{U_0 f_k}{2} + \frac{1}{2}\sum_{j=1}^{M'} (f_{j+k} + f_{|j-k|}) U_j .$$

This formula can be specialised to derive matrix representations for the products that involve the primary variables, provided that the expansion used for each base-flow quantity is appropriately chosen to have the odd or even parity that is needed to ensure a consistent treatment. For the products that involve the secondary variables, it is necessary to first apply the bidiagonal matrix that is inherent in the relationship between the primary and secondary variable coefficients that was previously stated in (17). The secondary variables can thus be eliminated by being represented entirely in terms of the primary variables. Composition with the appropriate product matrix then gives the required matrix representation. All of these representations, must in turn, also be composed with the matrices that specify the integration operators given by (13). However, this last stage in the construction of the linear operators is relatively straightforward, since as has already been noted, the integral operators all exhibit a narrowly banded matrix structure.

2.6. Solution of the eigenproblem

The discretisation that has been outlined can be cast into the form

$$\mathbf{A}(\alpha, \beta, \omega; R)\,\mathbf{p} = 0, \tag{23}$$

where $\mathbf{A}$ is a $3M \times 3M$ square matrix and $\mathbf{p}$ is the vector comprised of the $3M$ Chebyshev coefficients that represent the three primary variables. The matrix is quadratic in the spatial wavenumbers α, β and linear with respect to the temporal frequency ω. Notionally at least, the eigenproblem establishes the dispersion relation

$$\mathcal{D}(\alpha, \beta, \omega; R) = 0 \,, \tag{24}$$

where $\mathcal{D} = \det(\mathbf{A})$. In general, α and ω may take complex-values, but the cylindrical geometry constrains β to be real. The special case where α is real and ω is allowed to be complex is known as the temporal eigenvalue problem. However, the case where ω is prescribed to be real and α can then be taken to be complex is often of more physical interest, since it can be used to describe the behaviour of spatially developing waves that are excited using a localised time-periodic forcing [29]. This leads to the so-called spatial eigenvalue problem. Either way, the eigenproblem (23) can be solved using the eigenvalue routines that are available in standard software libraries for linear algebra. A value for the Reynolds number R must be selected and then two out of the three modal quantities α, β, ω prescribed, thus treating them as parameters for the determination of the one that remains.

2.7. Results and validation

Before presenting any numerical results, we remark that in obtaining our velocity-vorticity version of the equations for normal-mode disturbances, the parallel flow approximation is applied at a different stage in the derivation than in a number of earlier studies [7,8,19,24]. However, these previous investigations were not amongst themselves conducted in an entirely uniform fashion. Changes in the step at which terms involving radial derivatives were approximated led some small terms to be either retained or omitted. None of this would be expected to lead to any alterations that are of physical significance,

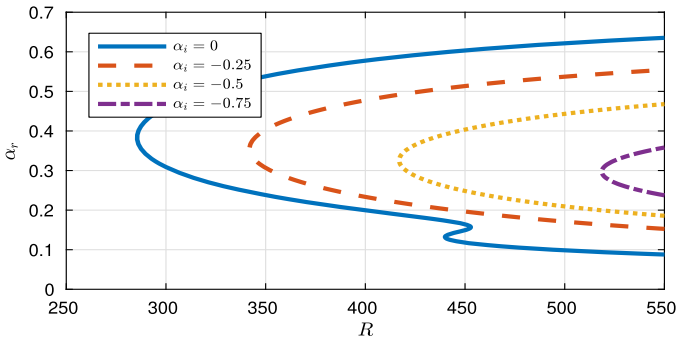

Fig. 1. Spatial growth rate contours for stationary ($\omega = 0$) disturbances. The solid line corresponds to the neutral curve $\alpha_i = 0$, while the successive enclosed dashed curves represent increasing levels of instability with $\alpha_i = -0.025, -0.05, -0.075$ respectively.

Table 1
Eigenvalue validation for the steady rotating disk boundary layer.

Critical parameters for stationary ($\omega = 0$) disturbances				
Mode	Reference	R_c	β_c	α_c
Type I	Malik [23]	285.36	0.07759	0.38402
	Cooper & Carpenter [7]	285.36	0.0776	0.38451
	Appelquist [1]	286.05	0.0776	0.38338
	Garrett et al. [15]	286.05	0.0775	0.38419
	This paper	**285.55**	**0.0772**	**0.3818**
Type II	Malik [23]	440.88	0.04672	0.13228
	Cooper & Carpenter [7]	440.87	0.0466	0.13159
	Appelquist [1]	452.97	0.0468	0.13227
	Garrett et al. [15]	450.95	0.04634	0.13067
	This paper	**439.95**	**0.0468**	**0.13186**

since the consequent variations amongst computed eigenvalues can be anticipated to be at most $O(1/R)$. This expectation is consistent with what was found in our own results. There are other more mundane sources for the slight discrepancies between previously published results, including such matters as whether only integer values of the azimuthal mode number n were allowed, rather than treating $\beta = n/R$, and therefore n, as continuously varying [15].

Fig. 1 shows radial growth rate contours that we have computed for the case of stationary ($\omega = 0$) forms of disturbance to the steady rotating disk boundary layer. The curves were determined for prescribed values of α_i using an arclength continuation method [14], in conjunction with a local iteration scheme [5], which tackled the quadratic dependency upon α that appears in the eigenvalue problem. The neutral ($\alpha_i = 0$) curve was found to coincide very closely with what had been calculated by previous investigators [8,19,23]. Extensive eigenvalue datasets were provided to us by the author of [1], which were used to conduct further stringent validation. We also considered the more general case of travelling wave forms of disturbance, but in the interests of brevity the details of all of the checks that were completed [25] are not presented here. It may be noted that, for the range of Reynolds numbers that were considered, it was typically necessary to use a Chebyshev series which was truncated with $M = 48$, in order to obtain numerical convergence for the computed eigenvalues.

Table 1 gives an overview of previously published results relating to the critical parameters for the onset of both type I and type II instabilities. These results are compared with those that were obtained in the current work. It can be seen that there is a very good measure of agreement, bearing in mind the potential for slight variations in the results that was discussed earlier. For each of the two types of instability, the temporal frequency ω_r was prescribed to be vanishing, while the critical values of α, β and R were found using interpolation near to the position where it was possible to identify a turning point in the variation of α with respect to the Reynolds number.

3. Linear stability of temporally periodic two dimensional flow configurations

We will now illustrate the application of our velocity-vorticity formulation and numerical solution methods to a temporally periodic flow scenario, by considering the Stokes layer that is generated by the motion of an infinitely long and flat rigid wall. The wall is located at $z^* = 0$ and oscillates along the x^*-direction in its own plane with a velocity $U_w^* \cos(\phi^* t^*)$, beneath an unbounded body of viscous fluid that would otherwise remain stationary. The constant boundary layer thickness is given by $\delta_s^* = \sqrt{2\nu^*/\phi^*}$ and this can be used to define a Reynolds number associated with the flow by setting

$$R = \frac{U_w^* \delta_s^*}{2\nu^*} = \frac{U_w^*}{\sqrt{2\nu^* \phi^*}}. \tag{25}$$

If all lengths are scaled using δ_s^* and we introduce a non-dimensional time $\tau = \phi^* t^*$, then in the absence of disturbances, the Stokes layer base flow is the unsteady unidirectional shear flow $\mathbf{U}_B = (U_B, 0, 0)$ given by

$$U_B(z,\tau) = e^{-z}\cos(\tau - z). \tag{26}$$

The development of disturbances to the basic flow can be studied using the two dimensional Cartesian version of the velocity-vorticity formulation that was introduced in section 2. Small-amplitude perturbations are specified by writing the total velocity and vorticity flow fields in the form

$$\mathbf{U}(x,z,\tau) = \mathbf{U}_B(z,\tau) + \mathbf{u}(x,z,\tau), \quad (\nabla\times\mathbf{U})(x,z,\tau) = (\nabla\times\mathbf{U}_B)(z,\tau) + \boldsymbol{\xi}(x,z,\tau), \tag{27}$$

where $\mathbf{u} = (u, 0, w)$ and $\boldsymbol{\xi} = \nabla\times\mathbf{u} = (0, \xi, 0)$. This leads to the linearised governing equations

$$\frac{1}{R}\frac{\partial\xi}{\partial\tau} + U_B\frac{\partial\xi}{\partial x} + U_B''w = \frac{1}{2R}\left(\frac{\partial^2}{\partial x^2} + \frac{\partial^2}{\partial z^2}\right)\xi \tag{28a}$$

$$\left(\frac{\partial^2}{\partial x^2} + \frac{\partial^2}{\partial z^2}\right)w = -\frac{\partial\xi}{\partial x}, \tag{28b}$$

for the primary variables $\{\xi, w\}$, whilst the secondary variable u is defined by the integral relation

$$u = -\int_z^\infty \left(\xi + \frac{\partial w}{\partial x}\right)dz'. \tag{29}$$

The constraints on the perturbations at the wall are given by

$$w(0) = 0, \qquad \int_0^\infty \left(\xi + \frac{\partial w}{\partial x}\right)dz' = 0, \tag{30}$$

where the imposition of no-slip has again been recast as an integral condition that must be satisfied by the vorticity, except that there is now only a single component of vorticity to determine. The perturbations also need to meet the far field vanishing requirements that $w, \xi \to 0$ for $z \to \infty$, but this behaviour is once more built directly into the Chebyshev discretisation.

3.1. Floquet stability equations

Because the base flow under consideration is no longer time independent, we cannot use the steady-state eigenvalue method that was deployed in section 2. It will be seen that this considerably increases the computational costs that are expended, since the temporal dependence of the perturbations cannot be prescribed to have a normal mode form. Instead, it is only possible to simplify the time-evolution of the disturbances by applying a decomposition based on Floquet theory [3,4,17]. We thus assume a so-called Floquet mode solution and write the primary variables in the general form

$$p(x,z,\tau) = e^{\mu\tau}\,\tilde{p}(z,\tau)\,e^{i\alpha x}, \tag{31}$$

where the profile function $\tilde{p}(z,\tau)$ is time-periodic with the same period as that of the wall oscillation. This means that it becomes necessary to determine the time-dependency of the disturbance profiles, in addition to their wall-normal variation. The temporal growth that develops over successive oscillation periods is incorporated into the exponential factor $e^{\mu\tau}$. Clearly the quantities of most interest will be $\mu_r = \Re(\mu)$ and $\alpha_i = \Im(\alpha)$, since these specify the temporal and spatial growth rates of the disturbances and can hence be used to determine whether or not there is stability. Attention will be restricted here to the case where the growth is taken to be purely temporal, for which α is chosen to be real-valued.

The time-periodic profile functions for the perturbation flow-fields, as well as the base flow itself, may be decomposed into harmonics such that

$$\tilde{p}(z,\tau) = \sum_{n=-\infty}^{\infty}\tilde{p}_n(z)e^{in\tau}, \qquad U_B(z,\tau) = u_1(z)e^{i\tau} + u_{-1}(z)e^{-i\tau}, \tag{32}$$

where $u_1 = \frac{1}{2}e^{-(1+i)z}$ and u_{-1} is its complex-conjugate. The infinite series must be truncated at an appropriate finite order N in order to obtain a numerical solution. This was first attempted by Hall [17] and then subsequently extended by Blennerhassett and Bassom [3,4] to achieve higher Reynolds numbers, which allowed the onset of instability to be identified. These studies all used a different formulation of the governing equations from our own, based on the natural generalisation of the Orr-Sommerfeld equation to the time-periodic case. The computational demands that ensue from an appropriate truncation of the harmonic series have been discussed at length elsewhere [3,4,34], so they will not be further examined

here. It suffices to say that, for a fixed wavenumber α, the previous studies required the use of a series representation with a large value of $N \sim \alpha R$ to obtain convergence, and this was found to be no different in our own investigations [25].

Substitution of the Floquet mode form (31) and the truncated version of the harmonic series (32) into the linearised governing equations (28) gives rise to a system of $2N+1$ coupled ordinary differential equations. These can then be addressed in a similar fashion to the equations that were considered in section 2 for the steady base-flow case. Just as before, the transformation (9) is used to map the semi-infinite physical domain to a finite computational domain that is labelled using the wall-normal co-ordinate η. The governing equations are then divided by η^2 and integrated twice with respect to η to yield the system

$$\left(\mathbf{L}_1^n + \mu \mathbf{I}_2\right) \hat{\xi}_n + \mathbf{M} \hat{\xi}_{n-1} - \bar{\mathbf{M}} \hat{\xi}_{n+1} + \mathbf{P} \hat{w}_{n-1} - \bar{\mathbf{P}} \hat{w}_{n+1} = 0 \tag{33a}$$

$$i\alpha \mathbf{I}_2 \hat{\xi}_n - \left(\alpha^2 \mathbf{I}_2 + \mathbf{J}\right) \hat{w}_n = 0, \tag{33b}$$

where

$$\mathbf{L}_1^n = \frac{\alpha^2}{2} \mathbf{I}_2 - \frac{1}{2} \mathbf{J} + in \mathbf{I}_2, \quad \mathbf{M} = i\alpha R \mathbf{I}_2 u_1, \quad \mathbf{P} = 2iR \mathbf{I}_2 u_1 \,. \tag{34}$$

The integral operators $\mathbf{I}_2$ and $\mathbf{J}$ are the same as those given by (13) and overbars are used to denote complex-conjugation. We have again adopted the notation $\hat{p} = \tilde{p}/\eta^2$ to indicate that the wall-normal variation of the primary variable flow fields is represented using an odd Chebyshev series which has the factored form (10). Parity considerations then require that the base flow and its wall-normal second derivative are expressed in terms of even polynomials.

3.2. Discretisation and solution of Floquet eigenvalue problem

Using the same ingredients for the Chebyshev discretisation that were described within various subdivisions of section 2, the system of coupled system of equations that is stated above can used to specify a numerical eigenvalue problem. For example, the integral constraint on the vorticity, which was given in (30), can be imposed in the same manner as before. However, it now yields a set of conditions, which hold between the Chebyshev coefficients for ξ_n and those of w_n, for every distinct value of the harmonic number n. The operations that involve multiplication by the wall-normal profile $u_1(z)$ for the basic state can also be determined using the method described previously. However, there is no longer the need to eliminate any secondary variables, since the perturbation velocity component u does not make any appearance in the governing equations, other than indirectly through its role in the enforcement of no-slip.

Putting everything together, the fully-discretised version of the eigenvalue problem can be cast into the general form

$$\mathbf{A}(\alpha, \mu; R)\, \mathbf{p} = 0 \,, \tag{35}$$

where $\mathbf{p}$ is a vector that is comprised of the Chebyshev coefficients of the $2(2N+1)$ primary variable profile functions $\{\hat{\xi}_n, \hat{w}_n\}$ and $\mathbf{A}$ is a square matrix that has a quadratic dependency with respect to the wavenumber α, while the eigenvalue μ appears linearly. The deployment of a Chebyshev series representation of order M means that the matrix is of size $2M(2N+1) \times 2M(2N+1)$. Fortunately, it can be arranged into a block tridiagonal form, which can be seen from an inspection of (33). The individual blocks are of size $2M \times 2M$. This structure arises because the purely sinusoidal time-periodicity of the basic state ensures that the profiles for the n-th harmonic are only directly coupled to those with harmonic numbers $n \pm 1$. As a consequence, the efficient sparse matrix routines that are available in standard linear algebra software libraries can be deployed to considerably reduce the computational costs.

It should be noted that, as must always be the case, the Floquet theory formulation for an oscillatory flow with a 2π fundamental periodicity only determines the imaginary parts of the eigenvalues to modulo unity. In other words, for each eigenvalue μ, we can expect $\mu \pm im$ to also be an eigenvalue, for any integer m. Moreover, the symmetry of the basic state with respect to reversals in the flow direction means that there is no discrimination between positive and negative phase velocities for propagating waves that have the same temporal growth rate. This implies that if μ is an eigenvalue, then so is its complex conjugate $\bar{\mu}$. Taking into consideration both of these two general properties, searches for any unstable modes can be restricted the interval $\mu_i \in [0, 1/2]$.

3.3. Results and validation

Table 2 presents two examples of results that were found using our numerical solution procedures and compares them against existing data, taken from reports of earlier studies [3,4,27]. In each case, the Reynolds number R and the streamwise wavenumber α were prescribed, while the eigenvalue μ was calculated using the discretised version of the eigenproblem which is summarised in equation (35). Evidently for the cases shown, the differences between the results that we obtained and those determined in previous investigations are very small. The results that were first found by Blennerhassett and Bassom [3] are exactly reproduced. The slight disparities with the eigenvalues reported in Blennerhassett and Bassom [4] and Ramage [27] can be explained by the fact that both of these later studies were conducted using a finite-width plane channel configuration to approximate the semi-infinite Stokes layer.

Table 2
Eigenvalue validation for the oscillatory Stokes layer.

Stokes layer Floquet eigenvalue comparisons			
R	α	Reference	μ
800	0.3	Blennerhassett and Bassom [3]	$0.08174 + 0.35096$i
		Blennerhassett and Bassom [4]	$0.08238 + 0.34583$i
		Ramage [27]	$0.0824 + 0.3458$i
		This paper	**0.081743+0.350960i**
847.5	0.38	Blennerhassett and Bassom [3]	$0.67594 + 0.14806$i
		Blennerhassett and Bassom [4]	$0.67616 + 0.14881$i
		This paper	**0.675937 + 0.148056i**

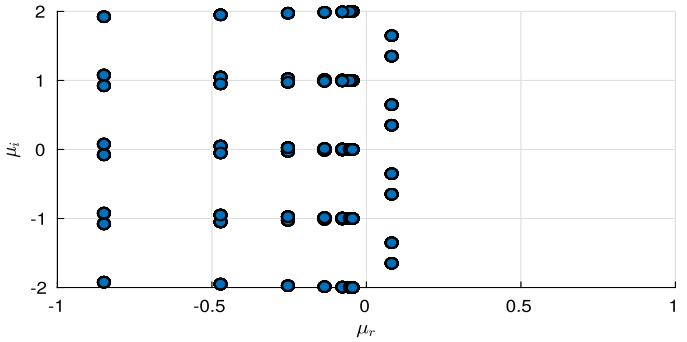

Fig. 2. Eigenvalue spectra of the semi-infinite Stokes layer for an unstable case where $R = 800$ and $\alpha = 0.3$.

Fig. 2 shows the numerically determined eigenvalue spectrum for the case with $R = 800$ and $\alpha = 0.3$. As has already been demonstrated in Table 1, the computation for the most unstable eigenvalue gives excellent agreement with previous work. But the figure is mainly of interest because it exhibits the expected eigenvalue repetition properties. Each eigenvalue is reproduced at intervals of $\Delta\mu = i$ as well as being mirrored by its complex conjugate.

Further details of the validation checks that were undertaken can be found in [25]. As can information concerning the choices for the discretisation parameters that ensured numerical convergence. Some measure of the computational demands that were made can be gained by noting the requirements for the particular instance that we have illustrated where $R = 800$. It proved necessary to set $N = 256$ in the truncated harmonic series which was used to represent the 2π-periodic component of the time variation, while employing Chebyshev series with order $M = 96$ to describe how the profiles varied across the boundary layer.

4. Linear stability of temporally periodic three dimensional flow configurations

In the previous two sections of this paper, we have presented our methods for conducting the linear stability eigenmodal analysis of three dimensional steady and two dimensional temporally periodic wall-bounded flows. These methods were exhibited and validated by considering two specific flow configurations that had previously been studied by other investigators. The goal of this section is to combine the numerical solution procedures that we have now described and apply them to a novel flow configuration, which is both three dimensional and temporally periodic. As was discussed in an introductory manner in section 1.3, we will analyse the stability behaviour for a rotating disk boundary-layer flow where there is a periodically modulated rate of rotation.

When the surface motion of the disk is prescribed to rotate the fluid in a time-varying manner, it remains possible to find a solution of the Navier-Stokes equations with the same relatively simple similarity structure as that which applies in the steady flow case. In what follows, we will consider examples where the previously constant rotation rate Ω^* is modified by a time-periodic modulation to become

$$\Omega^*_\epsilon(t^*) = \Omega^* + \epsilon\phi^* \cos(\phi^* t^*)\,. \tag{36}$$

As before, dimensional quantities are designated by an asterisk. The non-dimensional amplitude ϵ measures the range of the angular departures from the steadily rotating case, while ϕ^* specifies the temporal frequency with which they occur.

The velocity and lengths are non-dimensionalised in essentially the same fashion as they were in section 2.1. The same quantity as before, namely $\delta^* = \sqrt{\nu^*/\Omega^*}$, is used to provide a constant lengthscale. For a chosen reference radius r^*_L, the circumferential speed $r^*_L\Omega^*$ is again deployed to scale the velocities, though this now represents an average taken over time. The Reynolds number is once more specified by the definition given in equation (1), which means that it may still be interpreted as being the non-dimensional radius for the location at which it is defined. Retainment of the previously used scalings implies that, in the non-dimensionalised time τ, the underlying rotation period for the steady part of the disk

motion is $2\pi R$. The period of the oscillatory component is thus given by $2\pi R/\varphi$, where $\varphi = \phi^*/\Omega^*$ is the non-dimensional frequency that can be identified as the number of periods of modulation during one disk rotation.

Extending the previously considered similarity solution [37] to the unsteady case, the base flow can be written in the form

$$\mathbf{U}(r,z,\tau) = \left(\frac{r}{R}F(z,\tau), \frac{r}{R}G(z,\tau), \frac{1}{R}H(z,\tau)\right), \tag{37}$$

where F, G and H can be determined from the system of partial differential equations

$$\frac{\partial F}{\partial \tau} = \frac{1}{R}\left(F^2 - G^2 + H\frac{\partial F}{\partial z} - \frac{\partial^2 F}{\partial z^2}\right) \tag{38a}$$

$$\frac{\partial G}{\partial \tau} = \frac{1}{R}\left(2FG + H\frac{\partial G}{\partial z} - \frac{\partial^2 G}{\partial z^2}\right) \tag{38b}$$

$$\frac{\partial H}{\partial z} = -2F\,, \tag{38c}$$

which are subject to the boundary conditions

$$F(0,\tau) = H(0,\tau) = 0, \quad G(0,\tau) = 1 + \epsilon\varphi\cos\left(\frac{\varphi}{R}\tau\right) \tag{39a}$$

$$F \to 0, \qquad G \to 0 \quad \text{as} \quad z \to \infty\,. \tag{39b}$$

The required time-periodic solution of the system (38)–(39) was determined numerically, using a Chebyshev spectral discretisation for the variation in the direction normal to the disk surface, together with a predictor-corrector scheme for the time-marching. The temporal resolution was taken to be fine enough to facilitate an accurate decomposition of the time-variation of the base flow into a series of harmonics. This representation is needed for the subsequent Floquet stability analysis.

4.1. Floquet stability equations and eigenvalue problem

To consider the development of small disturbances to the unsteady base flow $\mathbf{U}_B$, we treat perturbations to the base flow in a similar fashion to section 3.1 and write

$$\mathbf{U}(r,\theta,z,\tau) = \mathbf{U}_B(r,z,\tau) + \mathbf{u}(r,\theta,z,\tau), \quad (\nabla\times\mathbf{U})(r,\theta,z,\tau) = (\nabla\times\mathbf{U}_B)(r,z,\tau) + \boldsymbol{\xi}(r,\theta,z,\tau)\,, \tag{40}$$

where the perturbation flow-fields are taken to have a Floquet-mode structure given by

$$p(r,\theta,z,\tau) = e^{\mu\tau}\,\tilde{p}(z,\tau)\,e^{i(\alpha r + n\theta)}\,. \tag{41}$$

The profile functions $\tilde{p}(z,\tau)$ are time-periodic with the same period $2\pi R/\varphi$ as that of the oscillatory base flow. As was the case before, the azimuthal mode number can be rewritten as $n = \beta R$ and allowed to take on a continuous set of values, whenever this is convenient. The incorporation of a normal-mode treatment for the radial variation, which introduces the radial wavenumber α, requires the application of a parallel flow approximation in the same manner as was discussed in section 2. For the purposes of conducting a locally-based modal analysis, the radial co-ordinate is again treated as if it were a parameter that can be identified with the Reynolds number.

The time-periodic profiles for the perturbation variables are represented using the truncated harmonic decomposition

$$\tilde{p}(z,\tau) = \sum_{n=-N}^{N} \tilde{p}_n(z) e^{in\left(\frac{\varphi}{R}\tau\right)}\,, \tag{42}$$

where the factor φ/R that appears in the exponents is needed to ensure that the series exhibits the same temporal periodicity as the basic state. The base flow is also described using a truncated series as

$$\mathbf{U}_B(z,\tau) = \sum_{n=-N_B}^{N_B} \mathbf{U}_n(z) e^{in\left(\frac{\varphi}{R}\tau\right)}\,. \tag{43}$$

It should be noted that in thus adopting a representation of the basic state as being independent of the radius, implicit use has been made of the parallel flow approximation. This amounts to setting $r = R$ in the similarity solution (37), at an appropriate stage in derivation of the governing equations for the perturbations.

In general, it is not necessary to take the same number of harmonics to represent the base flow and the disturbances. The series that are used for each of these can be anticipated to display different convergence behaviours. It may be recalled that for the example of the Stokes boundary layer, the base flow could be described exactly with $N_B = 1$. For the modulated

rotating disk configuration, it remains possible to utilise only a modest number of terms in the harmonic series to yield an adequate approximation of the base flow, provided that the amplitude parameter ϵ is taken to be sufficiently small. This can be traced to the quadratic nature of the nonlinearity that appears in (38), from which it may be anticipated that the amplitude of the n-th harmonic for the base flow will be of order $O(\epsilon^n)$.

Adapting the procedures that led to the systems (12) and (33) for the steady rotating disk boundary layer and the Stokes layer, respectively, we can derive the following coupled set of equations that can be used to determine the wall-normal variation for the harmonic components $\{\hat{\xi}_{rn}, \hat{\xi}_{\theta n}, \hat{w}_n\}$ of the three primary variables

$$\mathbf{I}_2\left[\left\{\mu + in\left(\frac{\varphi}{R}\right)\right\}\hat{\xi}_{rn} + i\beta\hat{N}_{zn} - \frac{2}{R}\left(\hat{\xi}_{\theta n} + i\alpha\hat{w}_n\right) + \frac{1}{R}\left(\alpha^2+\beta^2\right)\hat{\xi}_{rn}\right] + \frac{1}{l}\mathbf{I}_1\tilde{N}_{\theta n} - \frac{1}{Rl^2}\mathbf{J}\hat{\xi}_{rn} = 0 \tag{44a}$$

$$\mathbf{I}_2\left[\left\{\mu + in\left(\frac{\varphi}{R}\right)\right\}\hat{\xi}_{\theta n} - i\alpha\hat{N}_{zn} + \frac{2}{R}\left(\hat{\xi}_{rn} - i\beta\hat{w}_n\right) + \frac{1}{R}\left(\alpha^2+\beta^2\right)\hat{\xi}_{\theta n}\right] - \frac{1}{l}\mathbf{I}_1\tilde{N}_{rn} - \frac{1}{Rl^2}\mathbf{J}\hat{\xi}_{\theta n} = 0 \tag{44b}$$

$$\mathbf{I}_2\left(\left\{\frac{i\alpha}{R} - \alpha^2 - \beta^2\right\}\hat{w}_n - i\beta\hat{\xi}_{rn} + i\alpha\hat{\xi}_{\theta n} + \frac{1}{R}\hat{\xi}_{\theta n}\right) + \frac{1}{l^2}\mathbf{J}\hat{w}_n = 0. \tag{44c}$$

The integral operators $\mathbf{I}_1, \mathbf{I}_2, \mathbf{J}$ are unchanged from those that were specified in (13). The coupling between harmonics of different orders, which arises from multiplications with the time-dependent basic state, is comprised within the terms that are denoted as $\{\tilde{N}_{rn}, \tilde{N}_{\theta n}, \tilde{N}_{zn}\}$. Each of these can be expressed as a sum that takes the general form

$$N_n = \sum_{m=-N_B}^{N_B}\left(C_{rm}\,\hat{\xi}_{r\,n-m} + C_{\theta m}\,\hat{\xi}_{\theta\,n-m} + C_{wm}\,\hat{w}_{n-m}\right), \tag{45}$$

where the coupling functions C_{rm}, $C_{\theta m}$, C_{wm} can all be determined in terms of the m-th harmonic components $\mathbf{U}_m$ of the base flow that are given in the series (43). The use of an order N_B harmonic truncation to describe the base flow can be seen to establish direct linkages between the n-th order perturbation harmonics and those that have harmonic numbers $n \pm m$ for $m = 1, 2, \ldots N_B$.

The remaining stages of the numerical discretisation are very similar to those that have been outlined before. The wall-normal variations of the primary variables are once more described using truncated series of odd Chebyshev polynomials. Matrix operations representing multiplications with the coupling functions can then be determined in the same manner as was done for the base-flow products that were considered previously. Likewise for the implementation of the no-penetration condition and the imposition of the no-slip conditions using integral constraints on the vorticity, which are again applied individually for each of the harmonic components. All of this leads to a fully-discretised version of the eigenproblem that can be cast into the general form

$$\mathbf{A}(\alpha, \beta, \mu; R, \epsilon, \varphi)\,\mathbf{p} = 0\,, \tag{46}$$

where $\mathbf{p}$ is now taken to be a vector that is comprised of the Chebyshev coefficients of the $3(2N+1)$ primary variable profile functions $\{\hat{\xi}_{rn}, \hat{\xi}_{\theta n}, \hat{w}_n\}$. The use of a Chebyshev series representation of order M to discretise the wall-normal variation has the consequence that the square matrix $\mathbf{A}$ is of size $3M(2N+1) \times 3M(2N+1)$. In essentially the same manner as was the case for the steadily rotating disk boundary layer, the matrix exhibits a quadratic dependence upon the spatial wavenumbers α, β, while remaining linear with respect to the temporal eigenvalue μ.

If N_B may be taken to be relatively small, as was the case for the results that will be reported in the next section, then the matrix $\mathbf{A}$ displays a banded block structure. There are $3M \times 3M$ sized matrices arranged along its diagonal and repeated N_B times on either side. This means that, at least for the temporal version of the eigenproblem, where the radial wavenumber α is prescribed to be real while the Floquet eigenvalue μ is allowed to be complex, sparse matrix routines can be readily utilised from standard numerical software libraries, just as they were for the Stokes layer. However, for the spatial formulation, where μ is chosen to be purely imaginary and complex values of α must be determined, the quadratic dependency of $\mathbf{A}$ upon α was less straightforward to accommodate and led to considerable increases in the computational demands. Thus when the spatial eigenproblem was repeatedly tackled in parametric studies, it proved more convenient to adopt a local iterative approach, rather than attempting to solve the global eigenvalue problem afresh for every chosen specification of the parameters. Further details can be found in [25].

4.2. Validation and illustrative results

The results that we have obtained using our numerical solution of the eigenproblem for the rotating disk boundary layer with a modulated rate of rotation are novel, so they cannot be directly compared with any data provided from previous investigations, except for the limiting case where $\epsilon = 0$ for the modulation amplitude. However, it was still possible to conduct a number of careful validation checks, by making comparisons with results that were independently determined using alternative treatments of the disturbance behaviour.

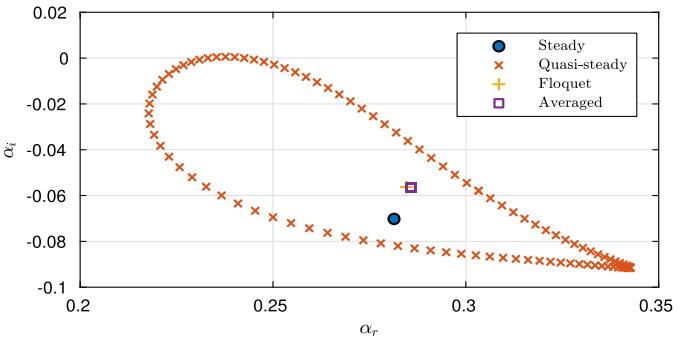

Fig. 3. Variation with the temporal oscillation phase for the complex-valued radial wavenumber α, determined using a quasi-steady approximation. The disturbances are stationary ($\mu = 0$ or $\omega = 0$) with $n = 32$ at $R = 500$, for $\epsilon = 0.02$ and $\varphi = 10$. The time-average is compared with the results obtained using Floquet theory and for the unmodulated steady case.

A quasi-steady formulation was applied to compute local-in-time versions of the Floquet eigenvalues. This approach relies upon a so-called frozen flow approximation, analogous to the parallel flow approximation, where the time variation of the oscillatory basic state is treated parametrically. The Floquet-mode structure can then be replaced by the simpler normal-mode structure that was deployed for the steady rotating disk configuration. This allows the stability problem to be reconsidered in the form of a series of locally defined problems for a succession of different steady basic states, one for each phase in the cycle of oscillation. A high measure of consistency was found between the results that were obtained in this manner and those that were derived using the Floquet theory [25].

Fig. 3 provides an illustration of the level of agreement that was found. The temporal variation of the complex-valued radial wavenumber α is displayed over a full cycle of the base state oscillation, for the case of a stationary disturbance ($\mu = 0$). It can be seen that the plotted values form a closed loop, and thus exhibit the same time-periodicity as the underlying boundary layer. Such behaviour is not generally guaranteed for results that are determined using a quasi-steady analysis. In particular, temporal periodicity is not exhibited in the locally-defined eigenvalues that have been computed for unstable disturbances in the Stokes layer [21]. Nevertheless, in cases where periodicity is found, it can be anticipated that the time-averages of eigenvalues determined using the quasi-steady approximation will give good predictions for the results that are obtained using Floquet theory. Inspection of the two appropriately labelled data points in the figure confirms that this is true for the example that is being considered. It can also be seen, by comparing the spatial eigenvalue that was computed for the Floquet eigenproblem with that which was found for the steady base-flow case, that there is a stabilising effect from the modulation of the rotation. This is evidenced by the reduction in the spatial growth rate $-\alpha_i$ with which the disturbance would be expected to develop radially outwards.

We were also able to determine the disturbance evolution by making use of linearised direct numerical simulations. These were conducted with a slightly amended version of a well-established computer code, which had previously been carefully tested and deployed to investigate disturbances in both the steady rotating disk and the Stokes boundary layers [11, 12,35]. The use of direct numerical simulations enabled the time variation of the perturbations to be computed without any prior assumptions being made about its general form. In particular, there was no prescription of either a normal-mode or a Floquet-mode structure for the temporal development. Good agreement was discovered between the large-time behaviour displayed in the simulations and what had been predicted from a consideration of the most unstable Floquet mode. More details concerning the comparisons that were undertaken are reported in [25].

In order to illustrate the physical interest of the new linear stability results that we have been able to obtain, it is useful to define a Reynolds number that characterises the unsteady component of the base flow. As was the case when the Stokes layer was considered in section 3, the oscillation frequency ϕ^* can be utilised to determine a boundary layer thickness $\delta_s^* = \sqrt{2\nu^*/\phi^*}$ and we can thus specify a second Reynolds number by setting

$$R_s = \frac{\left(r_L^* \epsilon \phi^*\right) \delta_s^*}{2\nu^*} = \epsilon \sqrt{\frac{\varphi}{2}}\, R\,. \tag{47}$$

It may be conjectured that this must be constrained to lie below a critical value $R_c \sim 700$ to avoid triggering the onset of any instability that is akin to that which besets the Stokes layer [3].

Fig. 4 shows the modifications that are obtained in the neutral curve for stationary forms of disturbances, when the rotation rate is modulated with $\epsilon = 0.01$ and $\varphi = 20$. It can be seen that there is a relatively weak stabilising effect for both the Type I and Type II forms of instability. However, the flow control parameters have been chosen in a very conservative fashion to yield $R_s \sim 10 << R_c$ over the range of R considered the figure, with the aim of making it highly unlikely that any other form of instability is promoted. The amplitude of the modulation in the rotation rate has also been kept to a moderately low value of $\epsilon\varphi = 0.2$. More substantial stabilisations were obtained by relaxing these constraints, which is promising from the point of view of potential applications to the delay of laminar-turbulent transition. It may be recalled,

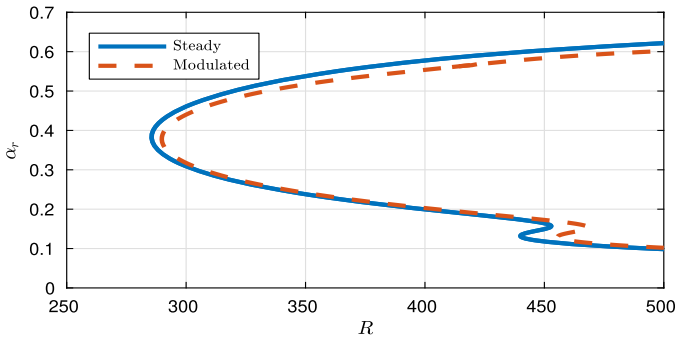

Fig. 4. Comparison between neutral curves for stationary disturbances ($\mu = 0$ or $\omega = 0$) in the steady case and a modulated case with control parameters $\epsilon = 0.01$, $\varphi = 20$.

from the introductory section, that stationary disturbances in the rotating disk boundary layer are destabilised by the same mechanism that generates stationary crossflow vortices in the flow over a swept wing.

To be assured that the computations that yielded the results that we have presented were numerically convergent, it was only necessary to truncate the harmonic series used to represent the basic state at $N_B = 2$, while the perturbation variables needed a harmonic series with $N = 5$. Just as was the case when the rotation rate was steady, the Chebyshev discretisation proved to be adequate with the deployment of $M = 48$ polynomials for each of the primary variables. Thus, in comparison to the Stokes layer stability problem, where we automatically have $N_B = 1$ but had typically required that $N = 256$ and $M = 96$, the computational demands were found to be relatively modest. However, this might be expected to change if it was decided to attempt to determine the onset of a Stokes layer type of instability in the modulated rotating disk boundary layer. A large separation between the timescales of the base state oscillation and those that characterise the perturbations could then develop, with the latter becoming very much shorter, giving rise to a substantial increase in the number of harmonics that would be needed to resolve them.

5. Conclusion

This paper describes novel methods for conducting a linear stability eigenmodal analysis for steady and temporally periodic boundary-layer flow configurations. A selection of exemplary flows are considered for the purposes of illustration. These are comprised of two cases of three dimensional boundary layers over disks that rotate with either a steady or a modulated rate, together with the two dimensional Stokes boundary layer formed above an oscillating plate. While we have only presented results for three dimensional base flows that could be formulated using a cylindrical polar coordinate system, the corresponding methodology for a Cartesian coordinate system should be evident.

A distinguishing feature of our approach, for the examples where the underlying flow is three dimensional, is that we use a velocity-vorticity formulation which consists of three coupled second-order equations that determine three primary variables [11]. These represent the perturbations to the wall-normal velocity component and the two vorticity components aligned with the plane of the wall. The remaining components of the perturbation velocity and the vorticity are all explicitly defined in terms of the primary variables, in a manner which allows them to be readily eliminated using the Chebyshev discretisation methods that we have developed.

More significantly, our approach incorporates what we believe to be a particularly convenient and elegant method for imposing the no-slip conditions on the velocity field. These are recast in the form of fully-equivalent integral constraints on the primary variable vorticity components. In the context of our chosen discretisation for the wall-normal variation, it is shown that the integral constraints that we have adopted are no more difficult to implement than the no-penetration condition that needs to be imposed upon the wall-normal component of the velocity. This remains the case if the velocity-vorticity formulation is specialised to describe disturbances that develop in two dimensions, for which the required number of integral constraints reduces from two to one.

The validation of our solution procedures is exhibited by some careful comparisons with results that were obtained in previously published studies for the cases of the steady rotating disk boundary layer and the oscillatory Stokes layer. The final section of the paper addresses a time-periodic three dimensional boundary layer, which thus combines what were construed to be the defining features of the two canonical flows that we had considered first. The steady rotating disk boundary layer is modified so that it displays a time periodicity, by means of a modulation in the rotation rate. The illustrative results that are presented for this novel flow configuration demonstrate the potential for the stabilisation of crossflow vortices that is afforded by the introduction of an oscillatory flow component into the base flow. Only a small selection of values from the set of possible choices for the control parameters have been considered here. A future paper will report the more extensive parametric study that has been completed [25].

Declaration of competing interest

The authors declare that they have no known competing financial interests or personal relationships that could have appeared to influence the work reported in this paper.

Acknowledgements

This work was supported by the UK Engineering and Physical Sciences Research Council.

References

[1] E. Appelquist, Direct numerical simulations of the rotating-disk boundary-layer flow, PhD thesis, KTH Royal Institute of Technology, Stockholm, 2014.
[2] A.J. Bard, L.R. Faulkner, Electrochemical Methods: Fundamentals and Applications, John Wiley and Sons, 2000.
[3] P.J. Blennerhassett, A.P. Bassom, The linear stability of flat Stokes layers, J. Fluid Mech. 464 (2002) 393–410.
[4] P.J. Blennerhassett, A.P. Bassom, The linear stability of high-frequency oscillatory flow in a channel, J. Fluid Mech. 556 (2006) 1–25.
[5] T.J. Bridges, P.J. Morris, Differential eigenvalue problems in which the parameter appears nonlinearly, J. Comput. Phys. 55 (1984) 437–460.
[6] T.J. Bridges, P.J. Morris, Boundary layer stability calculations, Phys. Fluids 30 (1987) 3351.
[7] A.J. Cooper, P.W. Carpenter, The stability of rotating-disc boundary-layer flow over a compliant wall. Part 1. Type I and II instabilities, J. Fluid Mech. 350 (1997) 231.
[8] A.J. Cooper, J.H. Harris, S.J. Garrett, M. Özkan, P.J. Thomas, The effect of anisotropic and isotropic roughness on the convective stability of the rotating disk boundary layer, Phys. Fluids 27 (1) (2015) 1–16.
[9] C. Davies, P.W. Carpenter, Numerical simulation of the evolution of Tollmien-Schlichting waves over finite compliant panels, J. Fluid Mech. 335 (1997) 361–392.
[10] C. Davies, P.W. Carpenter, Instabilities in a plane channel flow between compliant walls, J. Fluid Mech. 352 (1997) 205–243.
[11] C. Davies, P.W. Carpenter, A novel velocity-vorticity formulation of the Navier-Stokes equations with applications to boundary layer disturbance evolution, J. Comput. Phys. 172 (1) (2001) 119–165.
[12] C. Davies, P.W. Carpenter, Global behaviour corresponding to the absolute instability of the rotating-disc boundary layer, J. Fluid Mech. 486 (2003) 287–329.
[13] S.H. Davis, The stability of time-periodic flows, Annu. Rev. Fluid Mech. 8 (1) (1976) 57–74.
[14] K.I. Dickson, C.T. Kelley, I.C.F. Ipsen, I.G. Kevrekidis, Condition estimates for pseudo-arclength continuation, SIAM J. Numer. Anal. 45 (1) (2007) 263–276.
[15] S.J. Garrett, A.J. Cooper, J.H. Harris, M. Özkan, A. Segalini, P.J. Thomas, On the stability of von Kármán rotating-disk boundary layers with radial anisotropic surface roughness, Phys. Fluids 28 (1) (2016).
[16] N. Gregory, J.T. Stuart, W.S. Walker, On the stability of three-dimensional boundary layers with application to the flow due to a rotating disk, Philos. Trans. R. Soc., Math. Phys. Eng. Sci. 248 (943) (1955) 155–199.
[17] P. Hall, The linear stability of flat Stokes layers, Proc. R. Soc. Lond. Ser. A, Math. Phys. Sci. 359 (1697) (1978) 151–166.
[18] W. Heisenburg, Über Stabilität und Turbulenz von Flüssigkeitsströmen, Ann. Phys. 379 (15) (1924) 577–627.
[19] R.J. Lingwood, Absolute instability of the boundary layer on a rotating disk, J. Fluid Mech. 299 (1995) 17–33.
[20] R.J. Lingwood, P.H. Alfredsson, Instabilities of the von Kármán boundary layer, Appl. Mech. Rev. 67 (3) (2015) 05.
[21] J. Luo, X. Wu, On the linear instability of a finite Stokes layer: instantaneous versus Floquet modes, Phys. Fluids 22 (2010) 054106.
[22] L.M. Mack, Linear stability theory and the problem of supersonic boundary-layer transition, AIAA J. 13 (3) (1975) 278–289.
[23] M.R. Malik, The neutral curve for stationary disturbances in rotating-disk flow, J. Fluid Mech. 164 (1986) 275–287.
[24] M.R. Malik, P. Balakumar, Non-parallel stability of rotating disk flow using PSE, in: M.Y. Hussaini, A. Kumar, C.L. Streett (Eds.), Instability, Transition, and Turbulence, in: ICASE NASA LaRC Series, Springer, New York, 1992, pp. 168–180.
[25] S. Morgan, Stability of Periodically Modulated Rotating Disk Boundary Layers, PhD thesis, Cardiff University, 2018.
[26] W.M'F. Orr, The stability or instability of the steady motions of a perfect liquid and of a viscous liquid. Part i: a perfect liquid, Proc. R. Ir. Acad., A Math. Phys. Sci. 27 (1907) 9.
[27] A. Ramage, Linear disturbance evolution in the semi-infinite Stokes layer and related flows, PhD thesis, Cardiff University, 2017.
[28] P. Ricco, Laminar streaks with spanwise forcing, Phys. Fluids 23 (2011) 064103.
[29] P.J. Schmid, D.S. Henningson, Stability and Transition in Shear Flows, Applied Mathematical Sciences, Springer, New York, 2001.
[30] D.T. Schwartz, T.J. Rehg, P. Stroeve, B.G. Higgins, Fluctuating flow with mass transfer induced by a rotating disk electrode with a superimposed time-periodic modulation, Phys. Fluids A, Fluid Dyn. 2 (2) (1990) 167–177.
[31] A. Sommerfeld, Ein beitrag zur hydrodynamischen erklärung der turbulenten flüssigkeitsbewegungen, in: Proc. 4th Intl. Congr. Math., III, 1908, pp. 116–124.
[32] C. Thomas, Numerical simulations of disturbance development in rotating boundary layers, PhD thesis, Cardiff University, 2007.
[33] C. Thomas, A.P. Bassom, P.J. Blennerhassett, C. Davies, The linear stability of oscillatory Poiseuille flow in channels and pipes, Proc. R. Soc. Lond., Ser. A, Math. Phys. Eng. Sci. (2011).
[34] C. Thomas, C. Davies, The effects of mass transfer on the global stability of the rotating-disk boundary layer, J. Fluid Mech. 663 (2010) 401–433.
[35] C. Thomas, C. Davies, A. Bassom, P.J. Blennerhassett, Evolution of disturbance wavepackets in an oscillatory Stokes layer, J. Fluid Mech. 752 (2014) 543–571.
[36] C. Thomas, C. Davies, Global linear instability of rotating-cone boundary layers in a quiescent medium, Phys. Rev. Fluids 4 (2019) 043902.
[37] T. von Kármán, Uber laminaire und turbulente reibung, Z. Angew. Math. Mech. 1 (1921) 233–252.
[38] J.R. Womersley, Method for the calculation of velocity, rate of flow and viscous drag in arteries when the pressure gradient is known, J. Physiol. 127 (3) (1955) 553–563.